



UNIVERSITATEA BABEŞ-BOLYAI
Facultatea de Matematică și Informatică



Babeş-Bolyai University Cluj-Napoca
Faculty of Mathematics and Computer Science
400084 Cluj-Napoca, CP 253, Romania

Scientific report

Project title: **Transfer de Masă și Căldură în Nanofluid**

(code: PN-III-P4-ID-PCE-2016-0036)

Period: July 2017 – December 2017

Objectives:

O1. Studiul punctului de stagnare a unei curgeri rotationale axisimetrice in nanofluid pe o suprafata ce se extinde/contracta folosind modelul matematic a lui Buongiorno

The novel concept of nanofluids, first introduced by Choi (1995), has been proposed as a route to surpassing the performance of heat transfer fluids currently available. He has shown that heat transfer can be enhanced by employing various techniques and methodologies, such as increasing either the heat transfer surface or the heat transfer coefficient between the fluid and the surface, that allow high heat transfer rates in a small volume. Nanofluids occur naturally in a wide range of scientific fields which, recently has attracted the attention of researchers from a diverse range of fields such as chemical and mechanical engineering, biology, nuclear reactors, solar ponds, geothermal reservoirs, solar collectors, crystal growth in liquids, electronic cooling, chemical processing, etc. It is worth mentioning that many references on nanofluids can be found in the books by Nield and Bejan (2013), and Shenoy et al. (2016), and in the review papers by Buongiorno (2006), Mahian et al. (2013), Myers et al. (2017), etc.

During the period July, 12th 2017 – December, 31st 2017 the following articles indexed in the Web of Science Database were published:

1. M.A. Sheremet, I. Pop and O. Mahian, Natural convection in an inclined cavity with time-periodic temperature boundary conditions using nanofluids: Application in solar collectors. *International Journal of Heat and Mass Transfer* 116 (2018) 751–761. **Impact factor for 2016: 3.458.**

During the period July, 12th 2017 – December, 31st 2017 the following articles indexed in the Web of Science Database were accepted/sent for publication:

2. Cornelia Revnic, Eiyad Abu –Nada, Teodor Grosan and Ioan Pop, Natural convection in a rectangular cavity filled with nanofluids: effect of variable viscosity. *International Journal of Numerical Methods for Heat and Fluid Flow* (accepted). **Impact factor for 2016: 1.713.**
3. M. Sheremet, I. Pop and A.V. Roşca, The influence of thermal radiation on unsteady free convection in inclined enclosures filled by a nanofluid with sinusoidal boundary conditions. . *International Journal of Numerical Methods for Heat and Fluid Flow*. **Impact factor for 2016: 1.713.**
4. Natalia C. Roşca, Alin V. Roşca, Ioan Pop, MHD stagnation-point flow and heat transfer of a nanofluid over a stretching/shrinking sheet with melting, convective heat transfer and second order slip. *Applied Mathematics and Computations* (sent for publication). **Impact factor for 2016: 1.738.**
5. Teodor Groşan, Mikhail A. Sheremet, Ioan Pop and Serban Rareş Pop, Double-diffusive natural convection in a differentially heated wavy cavity under thermophoresis effect, *AIAA Journal of Thermophysics and Heat Transfer* (sent for publication)). **Impact factor for 2016: 1.315**

During the period July, 12th 2017 – December, 31st 2017 the following takls were given to conferences:

6. Natalia C. Rosca, Cost Action CA15119 (NANOUP TAKE) for the 2nd Grant Period (Lisbon, Portugal, 9 to 12 October 2017), where She has presented the paper: Axisymmetric rotational stagnation point flow impinging radially a permeable stretching/shrinking surface in a nanofluid using Tiwari and Das model by Natalia C. Roşca and Ioan Pop.
7. Alin Rosca, Cost Action CA15119 (NANOUP TAKE) for the 2nd Grant Period (Lisbon, Portugal, 9 to 12 October 2017), where he has presented the paper: MHD oblique stagnation-point flow for a Boussinesquian nanofluid past a stretching/shrinking sheet using Buongiorno’s model by A. Borrelli, G. Giantesio, M.C. Patria, N.C. Roşca, A.V. Roşca and I. Pop.

During the period July, 12th 2017 – December, 31st 2017 the following articles are in progress:

8. Teodor Grosan, Ioan Pop, Flow and heat transfer over a permeable bi-axial stretching/shrinking sheet in a nanofluid.
9. J.H. Merkin, N.C. Rosca, A.V. Rosca, I. Pop, Nanofluid flow by a permeable stretching/shrinking cylinder.

10. M.A. Sheremet, I. Pop, A.C. Baytaş, Non-equilibrium natural convection in a differentially heated nanofluid cavity partially filled with a porous medium

11. M.A. Sheremet, I. Pop, Marangoni natural convection in a cubical cavity filled with a nanofluid: Buongiorno's nanofluid model

Paper 1. Natural convection in an inclined cavity with time-periodic temperature boundary conditions using nanofluids: Application in solar collectors.

In this paper, the natural convection of alumina-water nanofluid inside a square cavity with time-sinusoidal temperature is studied numerically. The domain of interest is an inclined square cavity having isothermal wall at $\bar{x} = L$, while temperature of the wall $\bar{x} = 0$ is changed as a sinusoidal function of time, other walls are adiabatic. Dimensionless governing equations formulated using stream function, vorticity and temperature are

$$\frac{\partial^2 \psi}{\partial x^2} + \frac{\partial^2 \psi}{\partial y^2} = -\omega \quad (1)$$

$$\frac{\partial \omega}{\partial \tau} + u \frac{\partial \omega}{\partial x} + v \frac{\partial \omega}{\partial y} = H_1 \sqrt{\frac{Pr}{Ra}} \left(\frac{\partial^2 \omega}{\partial x^2} + \frac{\partial^2 \omega}{\partial y^2} \right) + H_2 \left\{ \frac{\partial \theta}{\partial x} \cos(\alpha) - \frac{\partial \theta}{\partial y} \sin(\alpha) \right\} \quad (2)$$

$$\frac{\partial \theta}{\partial \tau} + u \frac{\partial \theta}{\partial x} + v \frac{\partial \theta}{\partial y} = \frac{H_3}{\sqrt{Ra \cdot Pr}} \left(\frac{\partial^2 \theta}{\partial x^2} + \frac{\partial^2 \theta}{\partial y^2} \right) \quad (3)$$

with the corresponding boundary conditions

$$\begin{aligned} \tau = 0: \quad & \psi = 0, \quad \omega = 0, \quad \theta = 0.5 \quad \text{at } 0 \leq x \leq 1, \quad 0 \leq y \leq 1; \\ \tau > 0: \quad & \psi = 0, \quad \frac{\partial \psi}{\partial x} = 0, \quad \theta = \sin(f\tau) \quad \text{at } x = 0, \quad 0 \leq y \leq 1; \\ & \psi = 0, \quad \frac{\partial \psi}{\partial x} = 0, \quad \theta = 0 \quad \text{at } x = 1, \quad 0 \leq y \leq 1; \\ & \psi = 0, \quad \frac{\partial \psi}{\partial y} = 0, \quad \frac{\partial \theta}{\partial y} = 0 \quad \text{at } y = 0, 1, \quad 0 \leq x \leq 1 \end{aligned} \quad (4)$$

In order to determine the total heat transfer rate, we need to define the local heat transfer rate along the left vertical wall by the local Nusselt number as follows $Nu = (k_{nf} / k_f)(-\partial \theta / \partial x)_{x=0}$. Thus, the

average \overline{Nu} Nusselt number is defined by $\overline{Nu} = \int_0^1 Nu \, dy$.

The governing equations (1)–(3) with corresponding initial and boundary conditions (4) have been solved numerically by finite difference method of the second order accuracy (Sheremet and Pop,

2015; Sheremet et al., 2014,2015). In order to validate the present numerical code, the experimental (Ho et al., 2010) and numerical (Saghir et al., 2016) results are compared with the present one. Values of \overline{Nu} for $\phi = 1\%$, $Ra = 7.74547 \times 10^7$ and $Pr = 7.0659$ are 32.2037 (Ho et al., 2010) and 30.657 (Shaghir et al., 2016). It can be clearly seen that the results obtained demonstrate that the present results are accurate. Streamlines and isotherms of the considered natural convection within a square cavity are presented in Figs. 1 and 2 for $Ra = 10^5$, $f = 0.05\pi$, $\alpha = 0$ with $\phi = 0.03$.

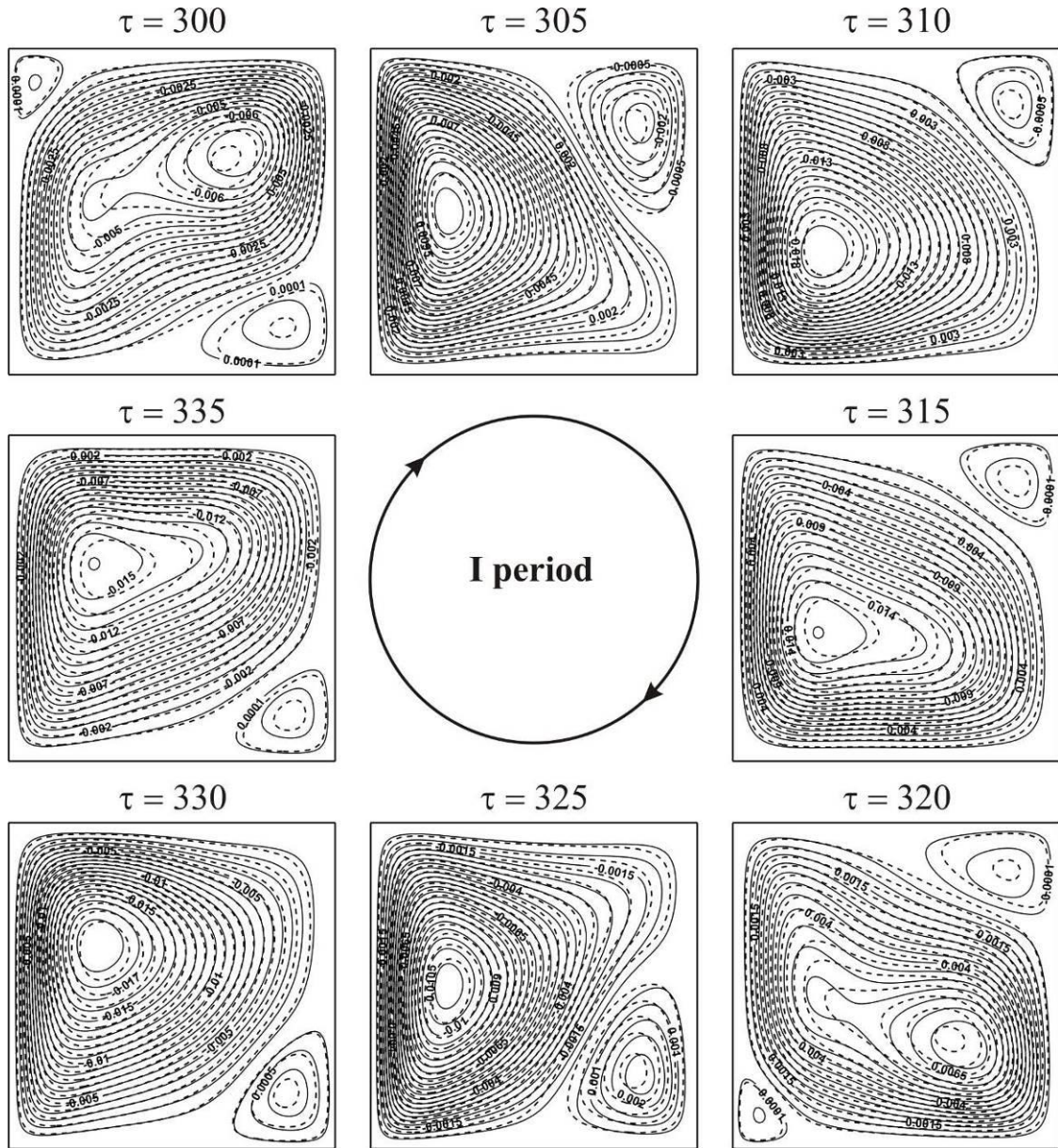


Fig. 1. Streamlines for a period of oscillations for $Ra = 10^5$, $f = 0.05\pi$, $\alpha = 0$ and $\phi = 0.0$ (solid lines), $\phi = 0.03$ (dashed lines)

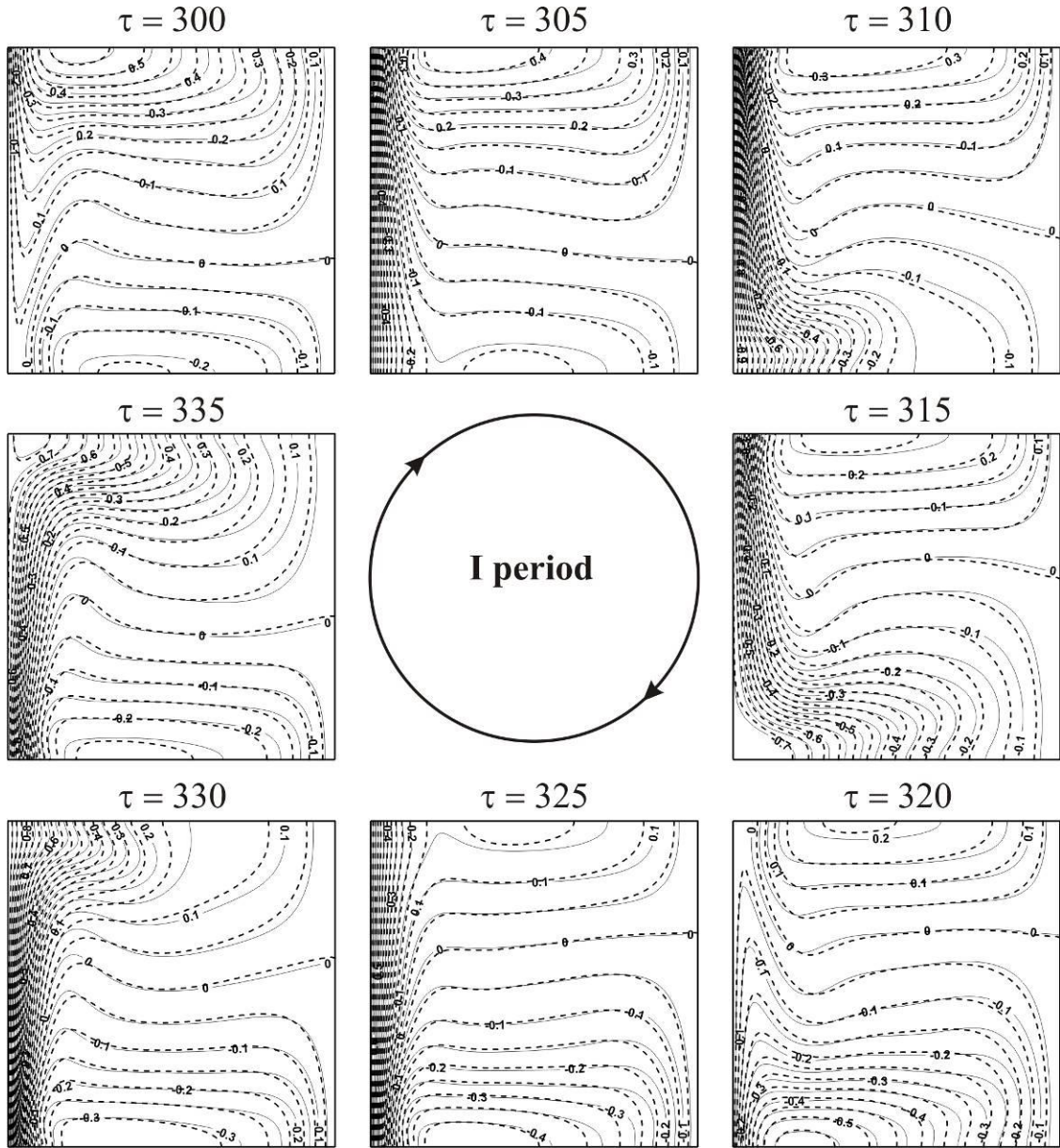


Fig. 2. Isotherms for a period of oscillations for $Ra = 10^5$, $f = 0.05\pi$, $\alpha = 0$ and $\phi = 0.0$ (solid lines), $\phi = 0.03$ (dashed lines)

Paper 2. Natural convection in a rectangular cavity filled with nanofluids: effect of variable viscosity

Consider the free convection in a two-dimensional square cavity filled with a CuO-water nanofluid. The height and the width of the enclosure are given by H and W , respectively. The left wall is heated and maintained at a constant temperature T_H , while the right wall is cooled and maintained at a constant temperature T_C where $T_H > T_C$, and the top and the bottom walls are considered

adiabatic. The nanoparticle flux $j_p = -\left(\rho_p D_B \nabla \bar{\varphi} + \rho_p D_T \frac{\nabla T}{T_C}\right)$ is assumed zero on the walls of the cavity. The thermal diffusivity, density, and heat capacitance of the nanofluid is written as:

$$\alpha_{nf} = \frac{k_{nf}}{(\rho C_p)_{nf}}, \quad \rho_{nf} = (1 - \varphi_b) \rho_f + \varphi_b \rho_p, \quad (\rho C_p)_{nf} = (1 - \varphi_b) (\rho C_p)_f + \varphi_b (\rho C_p)_p \quad (1)$$

where the symbol b denotes the average volume concentration of the nanoparticles in the enclosure. The effective thermal conductivity of the nanofluid k_{nf} is expressed by the model:

$$\frac{k_{nf}}{k_{bf}} = 1 + 64.7 \varphi_b^{0.7640} \left(\frac{d_{bf}}{d_p}\right)^{0.3690} \left(\frac{k_{bf}}{k_p}\right)^{0.7476} \text{Pr}_T^{0.9955} \text{Re}^{1.2321} \quad (2)$$

where Pr_T and Re are defined as: $\text{Pr}_T = \frac{\mu_f}{(\rho \alpha)_f}$, $\text{Re} = \frac{\rho_f k_b T}{3\pi \mu_f^2 l_f}$.

The governing equations in dimensionless form are given as:

$$\begin{aligned} \frac{\partial}{\partial x} \left(\omega \frac{\partial \psi}{\partial y} \right) - \frac{\partial}{\partial y} \left(\omega \frac{\partial \psi}{\partial x} \right) &= K_1 \left[\frac{\partial}{\partial x} \left(\mu \frac{\partial \omega}{\partial x} \right) + \frac{\partial}{\partial y} \left(\mu \frac{\partial \omega}{\partial y} \right) \right] + K_2 \left(\frac{\partial \theta}{\partial x} \right) + 4K_1 \left(\frac{\partial^2 \mu}{\partial x \partial y} \frac{\partial V}{\partial y} \right) \\ &+ K_1 \left(\frac{\partial^2 \mu}{\partial x^2} - \frac{\partial^2 \mu}{\partial y^2} \right) \left(\frac{\partial U}{\partial y} + \frac{\partial V}{\partial x} \right) + K_1 \left(\frac{\partial \mu}{\partial x} \frac{\partial \omega}{\partial x} + \frac{\partial \mu}{\partial y} \frac{\partial \omega}{\partial y} \right) \end{aligned} \quad (3)$$

$$\begin{aligned} \frac{\partial}{\partial x} \left(\theta \frac{\partial \psi}{\partial y} \right) - \frac{\partial}{\partial y} \left(\theta \frac{\partial \psi}{\partial x} \right) &= L_1 \left[\frac{\partial}{\partial x} \left(k \frac{\partial \theta}{\partial x} \right) + \frac{\partial}{\partial y} \left(k \frac{\partial \theta}{\partial y} \right) \right] \\ &+ L_2 \left(\frac{\partial \phi}{\partial x} \frac{\partial \theta}{\partial x} + \frac{\partial \phi}{\partial y} \frac{\partial \theta}{\partial y} \right) + L_3 \left[\left(\frac{\partial \theta}{\partial x} \right)^2 + \left(\frac{\partial \theta}{\partial y} \right)^2 \right] \end{aligned} \quad (4)$$

$$\frac{\partial}{\partial x} \left(\phi \frac{\partial \psi}{\partial y} \right) - \frac{\partial}{\partial y} \left(\phi \frac{\partial \psi}{\partial x} \right) = \frac{\text{Pr}}{\text{Sc}} \left[\frac{\partial^2 \phi}{\partial x^2} + \frac{\partial^2 \phi}{\partial y^2} + \frac{1}{N_{BT}} \left(\frac{\partial^2 \theta}{\partial x^2} + \frac{\partial^2 \theta}{\partial y^2} \right) \right] \quad (5)$$

$$\frac{\partial^2 \psi}{\partial x^2} + \frac{\partial^2 \psi}{\partial y^2} = -\omega \quad (6)$$

The boundary conditions for these equations are

$$1\text{- On the hot wall } x=0: \quad \psi = 0, \quad \omega = -\frac{\partial^2 \psi}{\partial x^2}, \quad \theta = 1, \quad J_p = 0$$

$$2\text{- On the cold wall } x=1: \quad \psi = 0, \quad \omega = -\frac{\partial^2 \psi}{\partial x^2}, \quad \theta = 0, \quad J_p = 0 \quad (7)$$

3- On the top and bottom walls $y = 1$ and $y = 0$: $\psi = 0$, $\omega = -\frac{\partial^2 \psi}{\partial x^2}$, $\frac{\partial \theta}{\partial y} = 0$, $J_p = 0$

For the first case, $\bar{\mu}_{\text{CuO}}(\bar{\varphi}, T)$ in dimensionless form is given by

$$\begin{aligned} \mu_{\text{CuO}}(\varphi, T) = & -0.6967 + \frac{15.937}{T_C + \Delta T \theta} + 1.238 \varphi_b \phi + \frac{1356.14}{(T_C + \Delta T \theta)^2} - 0.259 \varphi_b^2 \phi^2 \\ & - 30.88 \frac{\varphi_b \phi}{T_C + \Delta T \theta} - \frac{19652.74}{(T_C + \Delta T \theta)^3} + 0.01593 \varphi_b^3 \phi^3 + 4.38206 \frac{\varphi_b^2 \phi^2}{T_C + \Delta T \theta} \\ & + 147.573 \frac{\varphi_b \phi}{(T_C + \Delta T \theta)^2} \end{aligned} \quad (8)$$

respectively, for the second case,

$$\ln \mu_{\text{CuO}}(\varphi, T) = A \left(\frac{1}{T_C + \Delta T \theta} \right) - B, \quad (9)$$

where $A = 20587 \varphi_b^2 \phi + 15857 \varphi_b \phi + 1078.3$ and $B = -107.12 \varphi_b^2 \phi + 53.548 \varphi_b \phi + 2.8715$

The average Nusselt and Sherwood numbers are given by

$$Nu_{avg} = \int_0^1 Nu(y) dy, \quad Sh_{avg} = \int_0^1 Sh(y) dy \quad (10)$$

In order to solve the governing partial differential equations along with the boundary conditions we have used a central finite-difference discretization. The algebraic system obtained after discretization has been solved using the Gauss-Seidel iteration for uniform grid of different size. A mesh having 150x150 points is suitable for this problem and the following criteria were used to check the

convergence of the method $\frac{\|\Theta^{\text{new}} - \Theta^{\text{old}}\|}{\|\Theta^{\text{new}}\|} \leq \delta$ where Θ is either the variable ω , ψ , θ or ϕ , and δ

is a prescribed error, which, depends on the values of the governing parameters and was taken as 10^{-8} . The values of governing parameters are the Rayleigh number $Ra = 10^3, 10^4$ and 10^5 , the volume fraction $\varphi_b = 0.02$ and 0.05 and the difference between the hot and the cold wall is fixed to $10^0 C$. The temperature of cold and hot wall is taken as $T_c = 22^0 C, 40^0 C, 70^0 C$ and $T_h = 32^0 C, 50^0 C, 80^0 C$.

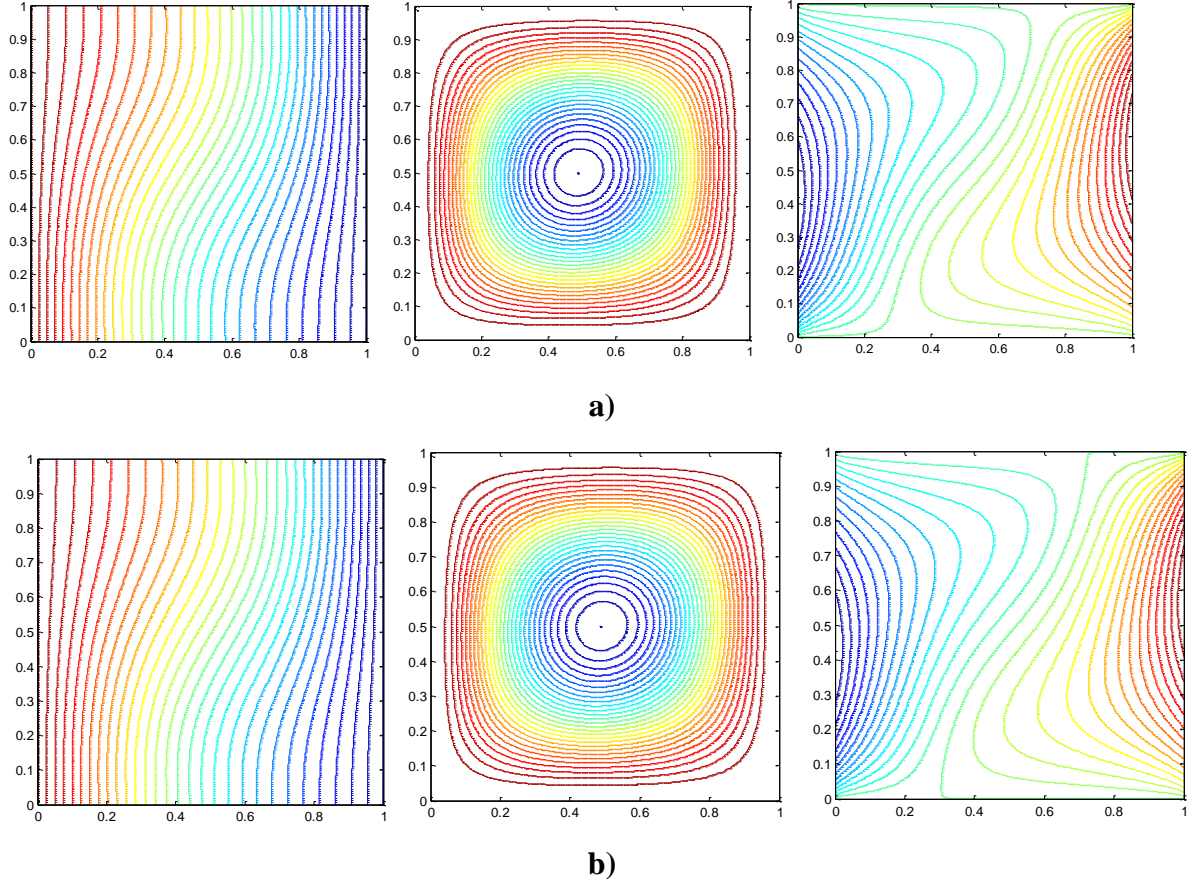


Fig. 1. Isotherms, streamlines and concentration lines for different volume fractions at $Ra = 10^3$
 $T_c = 22^\circ$, $T_h = 32^\circ$, a) $\phi_b = 0.02$, b) $\phi_b = 0.05$.

The influence of the volume fraction number ϕ_b on the isotherms, streamlines and volume concentration for the dynamic viscosity of nanofluid) and for temperature of hot and cold walls equal to $T_h = 32^\circ C$ and $T_c = 22^\circ C$ are displayed in Figs. 1 and 2. It is observed that when convection falls in the range $10^3 \leq Ra \leq 10^5$ the heat transfer from the hot to cold wall increases. Also, the fluid motion is augmented and the volume concentration patterns ϕ are strongly modified by the temperature distribution. Moreover, the single central vortex of streamlines at $Ra = 10^3$ (Fig. 1) present two vortices at $Ra = 10^5$ (Fig. 2). As it is seen in Fig.2, a higher-energy of nanoparticles transports through the flow become more clearly. In addition, for all the values of Ra , the central vortex of streamlines rotates clockwise as the volume fraction ϕ_b increases. The growth of the boundary layers increase with increasing of Ra .

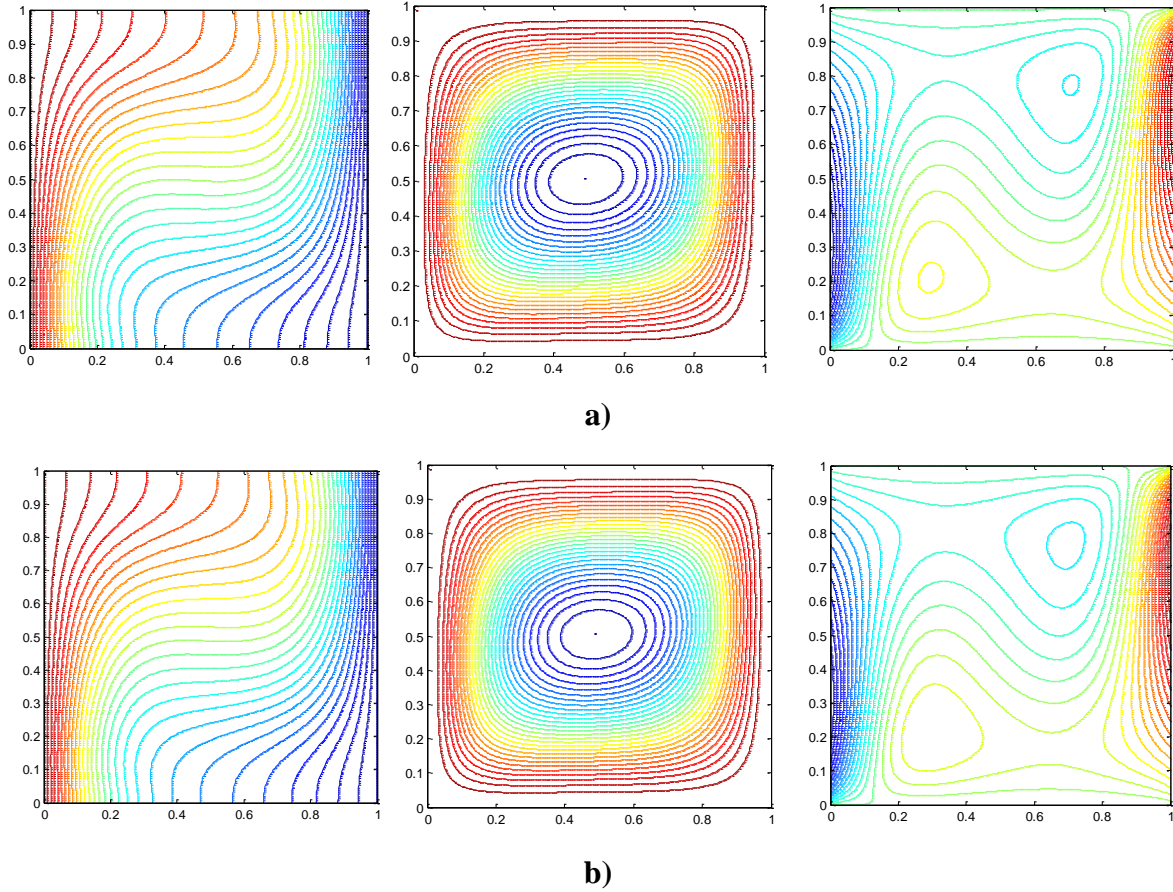


Fig. 2. Fig. 3 Isotherms, streamlines and concentration lines for different volume fractions at $Ra = 10^4$, $T_C = 22^\circ$, $T_h = 32^\circ$, a) $\phi_b = 0.02$, b) $\phi_b = 0.05$.

Paper 3. The influence of thermal radiation on unsteady free convection in inclined enclosures filled by a nanofluid with sinusoidal boundary conditions

1. Mathematical formulation of the problem

The physical model of free convection in an inclined square cavity filled with Al_2O_3 -water nanofluid and the coordinate system are schematically shown in Fig. 1. The domain of interest includes the nanofluid-filled cavity (shown in Fig. 1) with a sinusoidal temperature distribution along left wall. Horizontal walls are supposed to be adiabatic, while right vertical wall is kept at constant low temperature T_c . Temperature of left wall varies sinusoidally along y -coordinate. It is assumed in the analysis that the thermophysical properties of the fluid are independent of the temperature, and the flow is laminar.

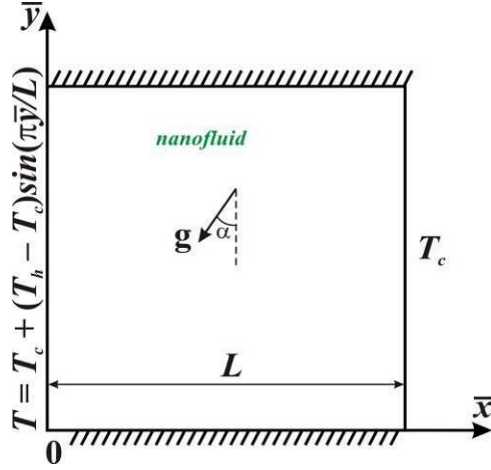


Fig. 1. A scheme of the system

The nanofluid is Newtonian and the Boussinesq approximation is valid. The base fluid and the nanoparticles are in thermal equilibrium. It is considered that viscous dissipation is neglected. Taking into account the abovementioned assumptions the governing equations can be written in dimensionless Cartesian variables as follows

$$\frac{\partial^2 \psi}{\partial x^2} + \frac{\partial^2 \psi}{\partial y^2} = -\omega \quad (1)$$

$$\frac{\partial \omega}{\partial \tau} + u \frac{\partial \omega}{\partial x} + v \frac{\partial \omega}{\partial y} = H_1 \sqrt{\frac{Pr}{Ra}} \left(\frac{\partial^2 \omega}{\partial x^2} + \frac{\partial^2 \omega}{\partial y^2} \right) + H_2 \left\{ \frac{\partial \theta}{\partial x} \cos(\alpha) - \frac{\partial \theta}{\partial y} \sin(\alpha) \right\} \quad (2)$$

$$\frac{\partial \theta}{\partial \tau} + u \frac{\partial \theta}{\partial x} + v \frac{\partial \theta}{\partial y} = \frac{H_3}{\sqrt{Ra \cdot Pr}} \left(\frac{\partial^2 \theta}{\partial x^2} + \frac{\partial^2 \theta}{\partial y^2} \right) \quad (3)$$

with the corresponding boundary conditions

$$\begin{aligned} \tau = 0: \quad & \psi = 0, \quad \omega = 0, \quad \theta = 0.5 \quad \text{at } 0 \leq x \leq 1, \quad 0 \leq y \leq 1; \\ \tau > 0: \quad & \psi = 0, \quad \frac{\partial \psi}{\partial x} = 0, \quad \omega = -\frac{\partial^2 \psi}{\partial x^2}, \quad \theta = \sin(\pi y) \quad \text{at } x = 0, \quad 0 \leq y \leq 1; \\ & \psi = 0, \quad \frac{\partial \psi}{\partial x} = 0, \quad \omega = -\frac{\partial^2 \psi}{\partial x^2}, \quad \theta = 0 \quad \text{at } x = 1, \quad 0 \leq y \leq 1; \\ & \psi = 0, \quad \frac{\partial \psi}{\partial y} = 0, \quad \omega = -\frac{\partial^2 \psi}{\partial y^2}, \quad \frac{\partial \theta}{\partial y} = 0 \quad \text{at } y = 0, 1, \quad 0 \leq x \leq 1 \end{aligned} \quad (4)$$

The physical quantities of interest are the local Nusselt number Nu along the sinusoidal temperature wall and the average Nusselt number \overline{Nu} , that are defined as

$$Nu = -\frac{k_{nf}}{k_f} \left(1 + \frac{4}{3} R_d \frac{k_f}{k_{nf}} \right) \frac{\partial \theta}{\partial x} \Big|_{x=0}, \quad \overline{Nu} = \int_0^1 Nu dy \quad (5)$$

2. Numerical procedure and results

The governing equations (1) to (3) with corresponding initial and boundary conditions (4) have been solved numerically by finite difference method of the second order accuracy. In order to validate the present numerical code, the experimental and numerical studies of natural convection of nanofluid in a differentially heated square cavity are considered.

A grid independency study was performed using five different grid sizes (50×50, 100×100, 200×200, 300×300 and 400×400) with $Ra = 10^5$, $Pr = 7.0$, $\phi = 0.03$, $R_d = 1$, $\alpha = 0$. The deviation of the average Nusselt numbers for 200×200, 300×300 and 400×400 is less than 0.5%. Hence, a grid size of 200×200 has been selected for obtaining the numerical results.

In the present study, we investigate transient natural convection of an alumina-water nanofluid in an inclined square cavity with a sinusoidal temperature profile along left vertical wall. The effects of the Rayleigh number ($Ra = 10^4-10^6$), inclination angle ($\alpha = 0-\pi/3$), nanoparticles volume fraction ($\phi = 0.0-0.04$) and radiation parameter ($R_d = 0-3$) on the fluid flow and heat transfer are examined for $Pr = 7.0$. The results are presented in the form of isotherms and streamlines, as well as average Nusselt number, and nanofluid flow rate. The streamlines and isotherms are plotted by solid and dashed lines for the clear fluid ($\phi = 0.0$) and nanofluid ($\phi = 0.04$), respectively.

Figure 2 presents an evolution of streamlines and isotherms for $Ra = 10^5$, $\alpha = 0$, $R_d = 1$ in the case of clear fluid (solid lines) and nanofluid with $\phi = 0.04$ (dashed lines). The considered domain of interest is a differentially-heated cavity, where temperature along the left vertical wall is changed from 0 at $y = 0$ till 0 at $y = 1$ using sinusoidal law $\theta = \sin(\pi y)$ with maximum value “1” at $y = 0.5$. At the same time, temperature along the right vertical wall is constant and has a minimum value “0” along this wall. Taking into account this horizontal temperature gradient and an influence of gravity force, convective flow evaluates inside the cavity. At $\tau = 1$ (Fig. 2a) we have heating from the left wall and cooling from the right one, as initial temperature is 0.5. Therefore, three convective cells are formed near the left wall, namely, one major circulation is located near the central part of this wall, where high temperature is kept and two minor circulations are formed at the left bottom and top corners of the cavity due to low temperature in these parts. One convective cell is formed close to the right wall. Temperature field illustrates a formation of isotherms near the isothermal vertical walls. A growth of time leads to a combination of two major convective cells with a displacement of the

obtained convective cell core, firstly, to the right part at $\tau = 3$ (Fig. 2*b*) and further to the central part at $\tau = 10$ (Fig. 2*e*). Isotherms reflect a formation of hot wave with ascending flows near the left wall and a cold wave with descending flows near the right vertical wall.

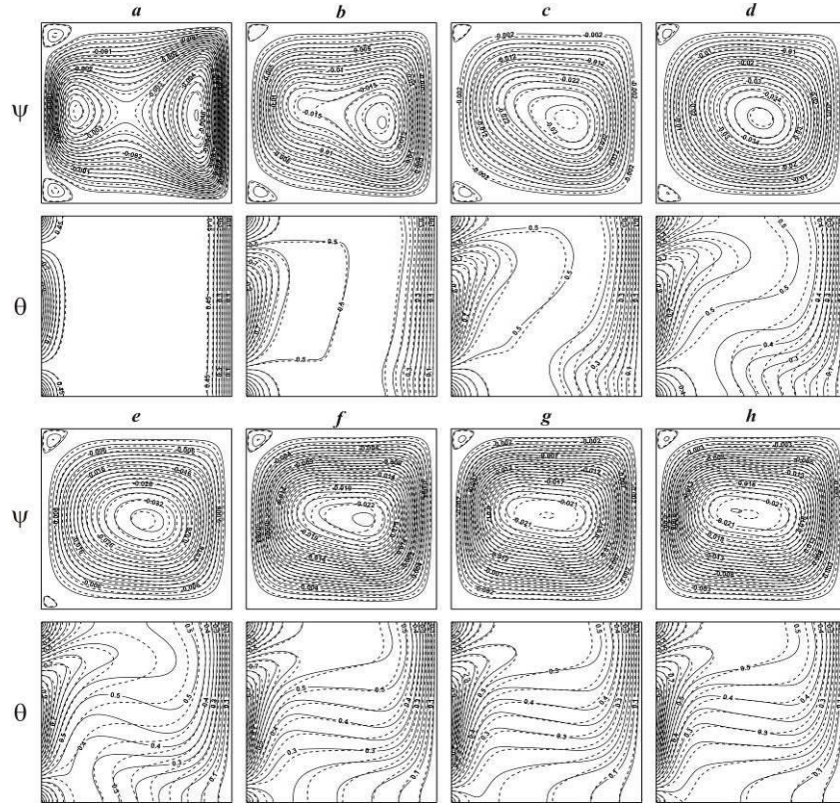


Fig. 2. Streamlines ψ and isotherms θ for $Ra = 10^5$, $\alpha = 0$, $R_d = 1$ and $\phi = 0.0$ (solid lines), $\phi = 0.04$ (dashed lines): $\tau = 1 - a$, $\tau = 3 - b$, $\tau = 5 - c$, $\tau = 7 - d$, $\tau = 10 - e$, $\tau = 20 - f$, $\tau = 50 - g$, $\tau = 200 - h$.

An increase in time $\tau > 10$ leads to a dissipating of a left bottom corner circulation due to a reduction of temperature gradient in this zone, when cold wave from the right wall interacts with a cold wave from this corner. For a steady state one can find one major central vortex with ascending flows near the left wall and descending flows close to the right wall, and one minor circulation located in the upper left corner. Distributions of isotherms illustrate a formation of two thermal boundary layers along vertical isothermal walls. Central part of the cavity characterizes a formation of temperature stratification core with heating from the upper part and cooling from the bottom one. Described flow and heat transfer behavior is similar for clear fluid and nanofluid. There are some differences in streamlines and isotherms due to more inertial flow of nanofluid with low effective viscosity. It should be noted that temperature stratification of clear fluid occurs earlier in comparison with a nanofluid.

Evolution of heat transfer and fluid flow rates are presented in Fig. 3 for different values of nanoparticles volume fraction. Evolution of average Nusselt number can be described as a change of three levels such as initial or heat conduction level with a reduction of \overline{Nu} due to heating of the surrounding fluid and as a result the temperature gradient decreases. The next level is a heat convection one, where average Nusselt number increases due to an intensive fluid flow and an interaction between hot and cold temperature waves with high temperature gradient. The final level is a steady state with constant value of average Nusselt number. The fluid flow rate reflects these levels for the flow structures. An increase in nanoparticles volume fraction leads to a reduction of average Nusselt number and fluid flow rate.

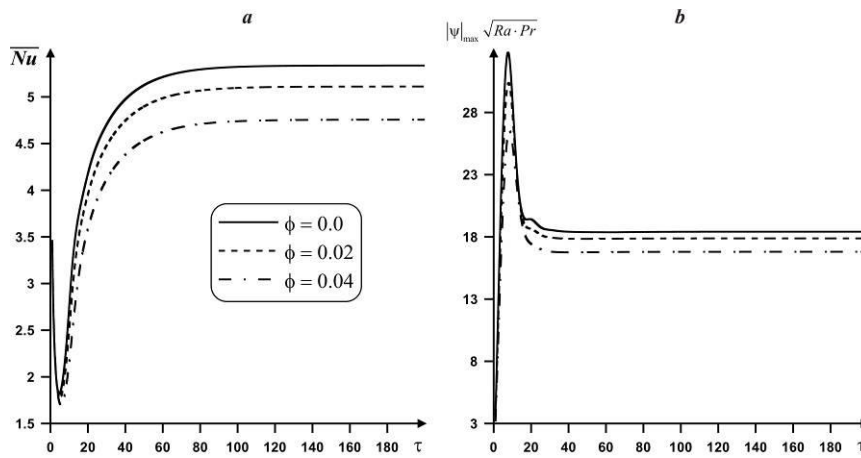


Fig. 3. Variations of average Nusselt number at left wall (a) and maximum absolute value of stream function (b) with time for $Ra = 10^5$, $\alpha = 0$, $R_d = 1$ and different values of nanoparticles volume fraction.

3. Conclusions

The transient natural convection and radiation heat transfer in an inclined square cavity filled with an alumina-water nanofluid has been investigated. The left thermal boundary condition is assumed to be a sinusoidal function of y -coordinate and the right one is kept at constant low temperature, while other walls are adiabatic. It has been found that an evolution of average Nusselt number and fluid flow rate can be described as a change of three levels such as initial or heat conduction level, heat convection level and steady state level. The average Nusselt number and fluid flow rate are increasing functions of the Rayleigh number and radiation parameter, and decreasing functions of nanoparticles volume fraction. A growth of the cavity inclination angle in the considered range leads to a rise of convective flow intensity, while the heat transfer rate is a nonlinear function of the cavity

inclination angle. It is possible to conclude that cavity inclination angle can be very good control parameters for heat and fluid flow inside the cavity.

Paper 4. MHD stagnation-point flow and heat transfer of a nanofluid over a stretching/shrinking sheet with melting, convective heat transfer and second order slip.

Consider the two-dimensional MHD stagnation-point flow of a water-based nanofluid past a stretching/shrinking sheet. The sheet is stretched/shrunk with the velocity $U_w(x)$, with fixed origin location, where x is the coordinate measured along the stretching/shrinking sheet, as shown in Fig. 1, while the velocity of the ambient (inviscid) fluid is $u_e(x)$. The nanofluid flows at $y \geq 0$, where y is the coordinate normal to the surface. It is assumed that the fluid is electrically conducted and a constant magnetic field B_0 is applied normal to the stretching/shrinking sheet. The magnetic Reynolds number is assumed small and so, the induced magnetic field can be considered to be negligible. It is also assumed that the constant temperature of the melting surface is T_m and that of the nanoparticle fraction is C_w , while that of the ambient fluid are T_∞ and C_∞ , respectively.

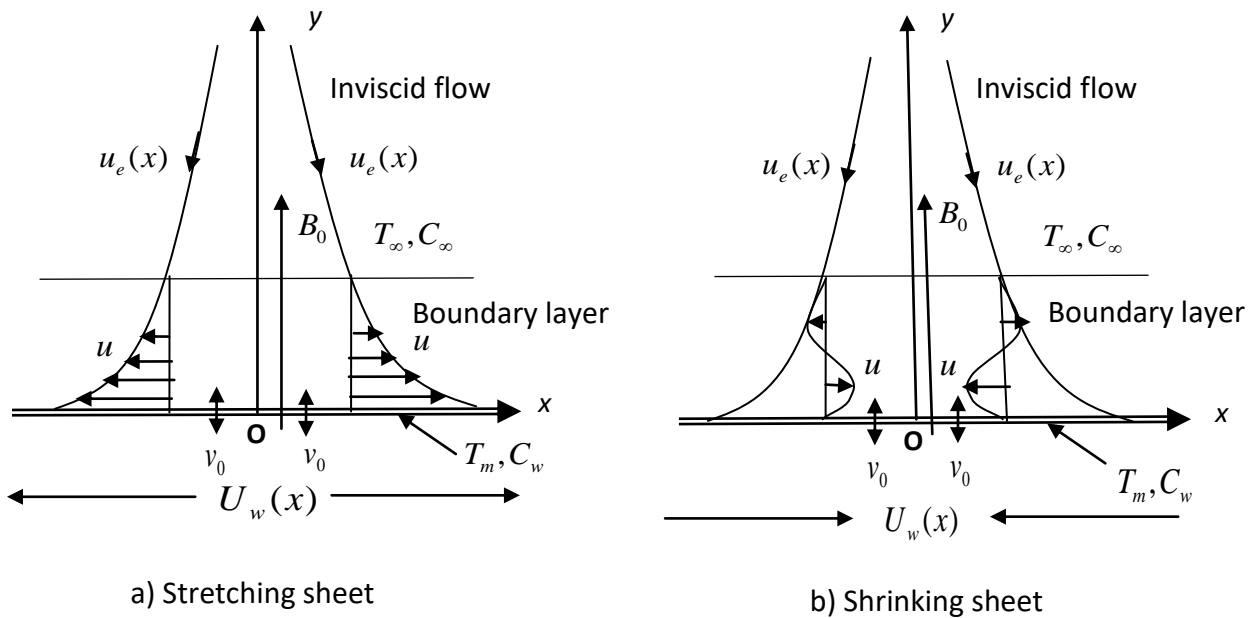


Fig. 1. Physical models and coordinate systems.

The governing boundary layer equations of continuity, momentum, thermal energy and nanoparticles are given in Cartesian coordinates as

$$\frac{\partial u}{\partial x} + \frac{\partial v}{\partial y} = 0 \quad (1)$$

$$u \frac{\partial u}{\partial x} + v \frac{\partial u}{\partial y} = u_e \frac{du_e}{dx} + v \frac{\partial^2 u}{\partial y^2} + \frac{\sigma B_0^2}{\rho} (u_e - u) \quad (2)$$

$$u \frac{\partial T}{\partial x} + v \frac{\partial T}{\partial y} = \alpha \frac{\partial^2 T}{\partial y^2} + \delta \left[D_B \frac{\partial C}{\partial y} \frac{\partial T}{\partial y} + \frac{D_T}{T_\infty} \left(\frac{\partial T}{\partial y} \right)^2 \right] \quad (3)$$

$$u \frac{\partial C}{\partial x} + v \frac{\partial C}{\partial y} = D_B \frac{\partial^2 C}{\partial y^2} + \frac{D_T}{T_\infty} \frac{\partial^2 T}{\partial y^2} \quad (4)$$

subject to the boundary conditions

$$\left. \begin{aligned} u(x) &= \lambda U_w(x) + u_{w,slip}(x), \quad v = v_0, \quad T = T_m \\ k \frac{\partial T}{\partial y} &= \rho [L + c_s (T_m - T_0)] v_0, \quad C = C_w \quad \text{at } y = 0 \end{aligned} \right\} \quad (5)$$

$$u \rightarrow u_e(x), \quad T \rightarrow T_\infty, \quad C \rightarrow C_\infty \quad \text{as } y \rightarrow \infty$$

Assuming that $U_w(x) = cx$ and $u_e(x) = cx$ with c a positive constant, we look for a similarity solution of Eqs. (1) to (4) subject to the boundary conditions (5) of the following form

$$\begin{aligned} u &= cx f'(\eta), \quad v = -\sqrt{c\nu} f(\eta), \quad \theta(\eta) = (T - T_m)/(T_\infty - T_m) \\ \phi(\eta) &= (C - C_\infty)/(C_w - C_\infty), \quad \eta = \sqrt{c/\nu} y \end{aligned} \quad (6)$$

where prime denotes differentiation with respect to η . Thus, we have

$$v_0 = -\sqrt{c\nu} S \quad (7)$$

where $S = -v_0/\sqrt{c\nu}$ is the constant mass flux parameter with $S > 0$ for suction and $S < 0$ for injection, respectively.

Substituting (6) into Eqs. (2) to (4), we obtain the following ordinary (similarity) differential equations

$$f'''' + f f'' + 1 - f'^2 + M(1 - f') = 0 \quad (8)$$

$$\frac{1}{Pr} \theta'' + f \theta' + Nb \phi' \theta' + Nt \theta'^2 = 0 \quad (9)$$

$$\phi'' + Sc f \phi' + \frac{Nt}{Nb} \theta'' = 0 \quad (10)$$

and the boundary conditions (5) become

$$f(0) = S, \quad f'(0) = \lambda + a f''(0) + b f'''(0), \quad Me\theta'(0) + PrS = 0, \quad \phi(0) = 1$$

$$f'(\eta) \rightarrow 1, \quad \theta(\eta) \rightarrow 1, \quad \phi(\eta) \rightarrow 0 \quad \text{as } \eta \rightarrow \infty \quad (11)$$

The physical quantities of interest are the skin friction coefficient C_f and the local Sherwood number Sh_x which are given by

$$Re_x^{1/2} C_f = f''(0), \quad Re_x^{-1/2} Sh_x = -\phi'(0) \quad (12)$$

where $Re_x = U_w(x)x/\nu$ is the local Reynolds number.

The system of coupled three ordinary differential equations (8) to (10) subject to the boundary conditions (11) was solved numerically using the function `bvp4c` from Matlab. Both the cases of stretching ($\lambda > 0$) and shrinking ($\lambda < 0$) sheets have been studied. The relative tolerance was set to 10^{-7} . The results are given for several values of the governing parameters and they are presented in Figs. 2 and 3 for several values of λ, M, a, b and S , when $Pr = 1, Nb = Nt = 0.1$ and $Sc = Me = 1$. These figures illustrate the variation of the reduced skin friction coefficient $f''(0)$ and reduced Sherwood number $-\phi'(0)$. We observe from these figures that the system of equations (8) to (10) subject to the boundary conditions (11) admits multiple (dual) solutions, i.e. one upper branch solution and one lower branch solution, respectively. From the performed stability analysis it follows that the upper branch solutions are stable and physically realizable, while the lower branch solutions are not stable and hence physically not realizable.

Figures 2 and 3 show that for both $f''(0)$ and $-\phi'(0)$ the dual solutions exist only for the shrinking sheets case. Here $\lambda_{c_i} < 0$ are the critical values of $\lambda < 0$ starting from which the system of equations (8) to (10) subject to the boundary conditions (11) has at least one solution. From Fig. 2 we notice that the reduced skin friction coefficient increases with M for the upper branch solution. From Fig. 3 we observe an asymptotic behavior of the reduced Sherwood number near the critical values for the lower branch solutions. Also, sample velocity, temperature and concentration profiles along both solution branches are graphically presented.

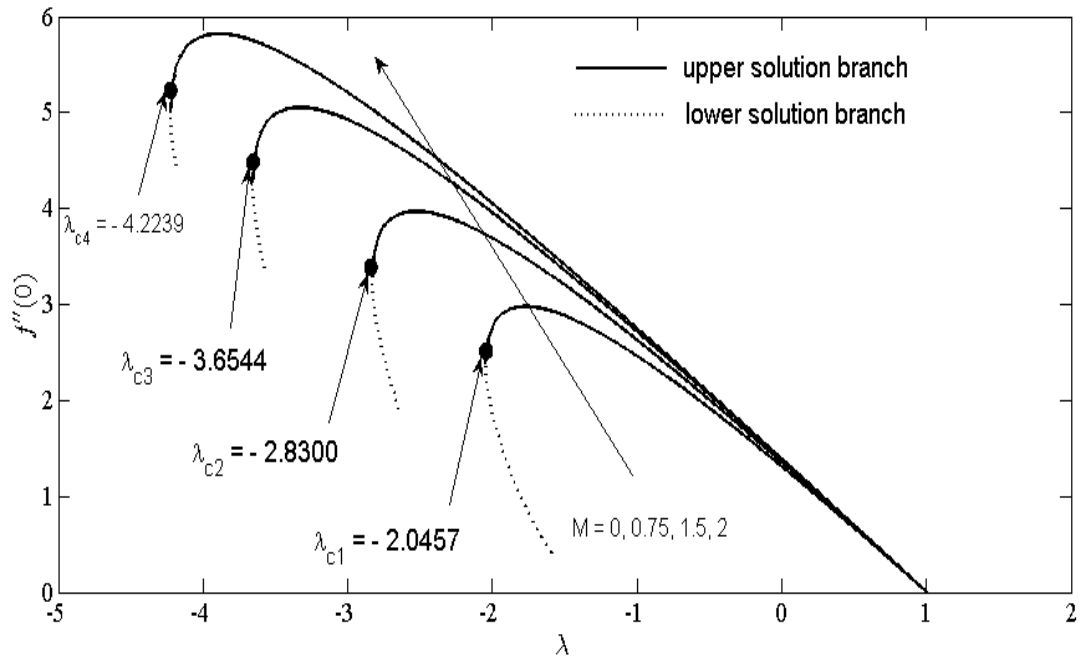


Fig. 2. Variation of $f''(0)$ with λ for several values of M when $S = 1$, $a = 0.1$ and $b = -0.1$.

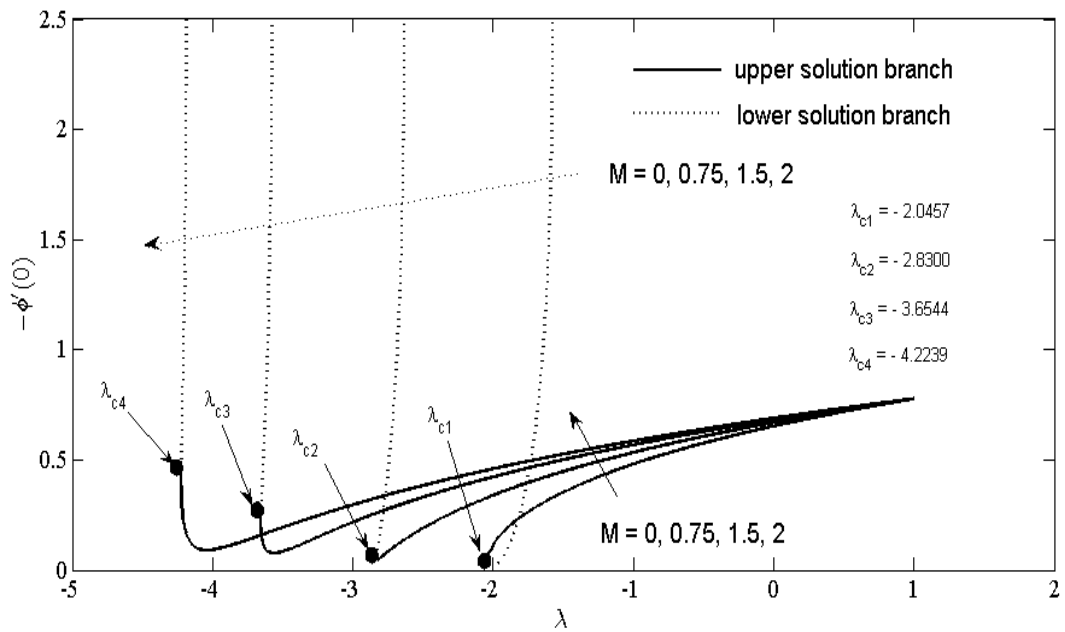


Fig. 3. Variation of $-\phi'(0)$ with λ for several values of M when $Pr = 1$, $Nb = Nt = 0.1$, $Sc = Me = 1$, $S = 1$, $a = 0.1$ and $b = -0.1$.

Paper 5. Double-diffusive natural convection in a differentially heated wavy cavity under thermophoresis effect

We analyze the free convective flow and heat transfer of a warm gas, containing suspended aerosol particles, inside a differentially heated square cavity with a wavy isothermal wall. The domain of interest is presented in Fig. 1. The considered enclosure is kept at constant temperatures T_1 and T_2 and constant concentrations C_1 and C_2 at the left wavy and right flat walls, while horizontal walls are adiabatic and impermeable.

Except for the density, the properties of the fluid are taken to be constant. It is further assumed that the effect of buoyancy is included through the Boussinesq approximation in the following form:

$$\rho = \rho_0 [1 - \beta_T (T - T_c) - \beta_C (C - C_c)].$$

Therefore the dimensionless equations can be written as follows

$$\frac{\partial^2 \psi}{\partial x^2} + \frac{\partial^2 \psi}{\partial y^2} = -\omega \quad (1)$$

$$\frac{\partial \omega}{\partial \tau} + u \frac{\partial \omega}{\partial x} + v \frac{\partial \omega}{\partial y} = \sqrt{\frac{Pr}{Ra}} \nabla^2 \omega + \frac{\partial \theta}{\partial x} + \beta \frac{\partial \phi}{\partial x} \quad (2)$$

$$\frac{\partial \theta}{\partial \tau} + \frac{\partial \psi}{\partial y} \frac{\partial \theta}{\partial x} - \frac{\partial \psi}{\partial x} \frac{\partial \theta}{\partial y} = \frac{1}{\sqrt{Ra \cdot Pr}} \left(\frac{\partial^2 \theta}{\partial x^2} + \frac{\partial^2 \theta}{\partial y^2} \right) \quad (3)$$

$$\begin{aligned} \frac{\partial \phi}{\partial \tau} + \frac{\partial \psi}{\partial y} \frac{\partial \phi}{\partial x} - \frac{\partial \psi}{\partial x} \frac{\partial \phi}{\partial y} &= \frac{1}{Sc} \sqrt{\frac{Pr}{Ra}} \left(\frac{\partial^2 \phi}{\partial x^2} + \frac{\partial^2 \phi}{\partial y^2} \right) + \\ &+ k_T \sqrt{\frac{Pr}{Ra}} \left\{ \frac{\partial}{\partial x} \left(\frac{\phi + N_C}{\theta + N_T} \cdot \frac{\partial \theta}{\partial x} \right) + \frac{\partial}{\partial y} \left(\frac{\phi + N_C}{\theta + N_T} \cdot \frac{\partial \theta}{\partial y} \right) \right\} \end{aligned} \quad (4)$$

with the following boundary conditions

$$\begin{aligned} \psi = 0, \quad \omega &= -\frac{\partial^2 \psi}{\partial x^2} - \frac{\partial^2 \psi}{\partial y^2}, \quad \theta = 1, \quad \phi = 1 \quad \text{on the left wavy wall} \\ \psi = 0, \quad \omega &= -\frac{\partial^2 \psi}{\partial x^2}, \quad \theta = 0, \quad \phi = 0 \quad \text{on the right flat wall} \\ \psi = 0, \quad \omega &= -\frac{\partial^2 \psi}{\partial y^2}, \quad \frac{\partial \theta}{\partial y} = 0, \quad \frac{\partial \phi}{\partial y} = 0 \quad \text{on the bottom and top walls} \end{aligned} \quad (5)$$

Here $Ra = g \beta_T \Delta T L^3 / (\nu \alpha)$ is the Rayleigh number, $Pr = \nu / \alpha$ is the Prandtl number, $\beta = \frac{\beta_C \Delta C}{\beta_T \Delta T}$ is

the buoyancy ratio parameter, $Sc = \nu / D$ is the Schmidt number, $N_C = \frac{C_c}{\Delta C}$ and $N_T = \frac{T_c}{\Delta T}$ are the

thermophoresis parameters, $\Delta C = C_h - C_c$ and $\Delta T = T_h - T_c$.

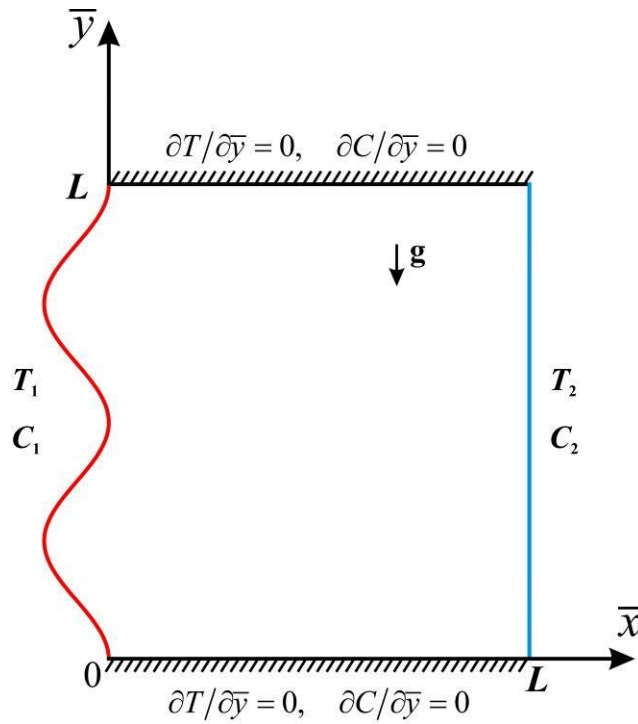


Fig. 1. Physical model and coordinate system

The physical quantities of interest are the local Nusselt number Nu and local Sherwood number along the hot wavy wall and average Nusselt number \overline{Nu} and average Sherwood number \overline{Sh} .

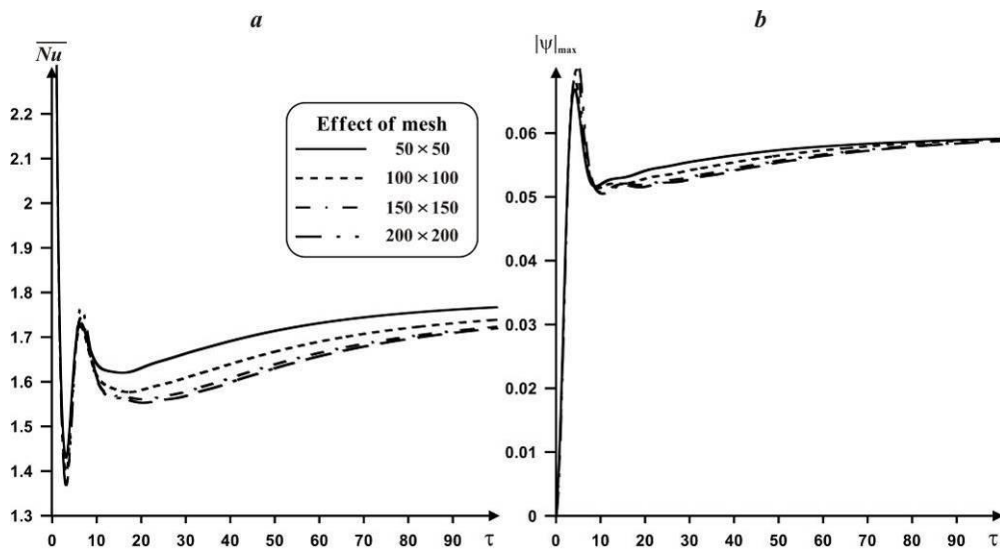


Fig. 2. Variation of the average Nusselt number of the left vertical wall (a) and fluid flow rate inside the cavity (b) versus the dimensionless time and the mesh parameters

The cavity in the x and y plane, i.e., physical domain, is transformed into a rectangular geometry in the computational domain using an algebraic coordinate transformation by introducing new independent variables ξ and η . The left and right walls of the cavity become coordinate lines having constant values of ξ . The independent variables in the physical domain are transformed to independent variables in the computational domain by the following equations:

$$\begin{cases} \xi = \frac{x-x_1}{\Delta} = \frac{x-1+a+b \cdot \cos(2\pi\kappa y)}{a+b \cdot \cos(2\pi\kappa y)}, \\ \eta = y \end{cases} \quad (6)$$

The governing equations with corresponding boundary conditions were solved using the finite difference method of the second order accuracy. For the purpose of obtaining grid independent solution, a grid sensitivity analysis is performed (see Fig. 2).

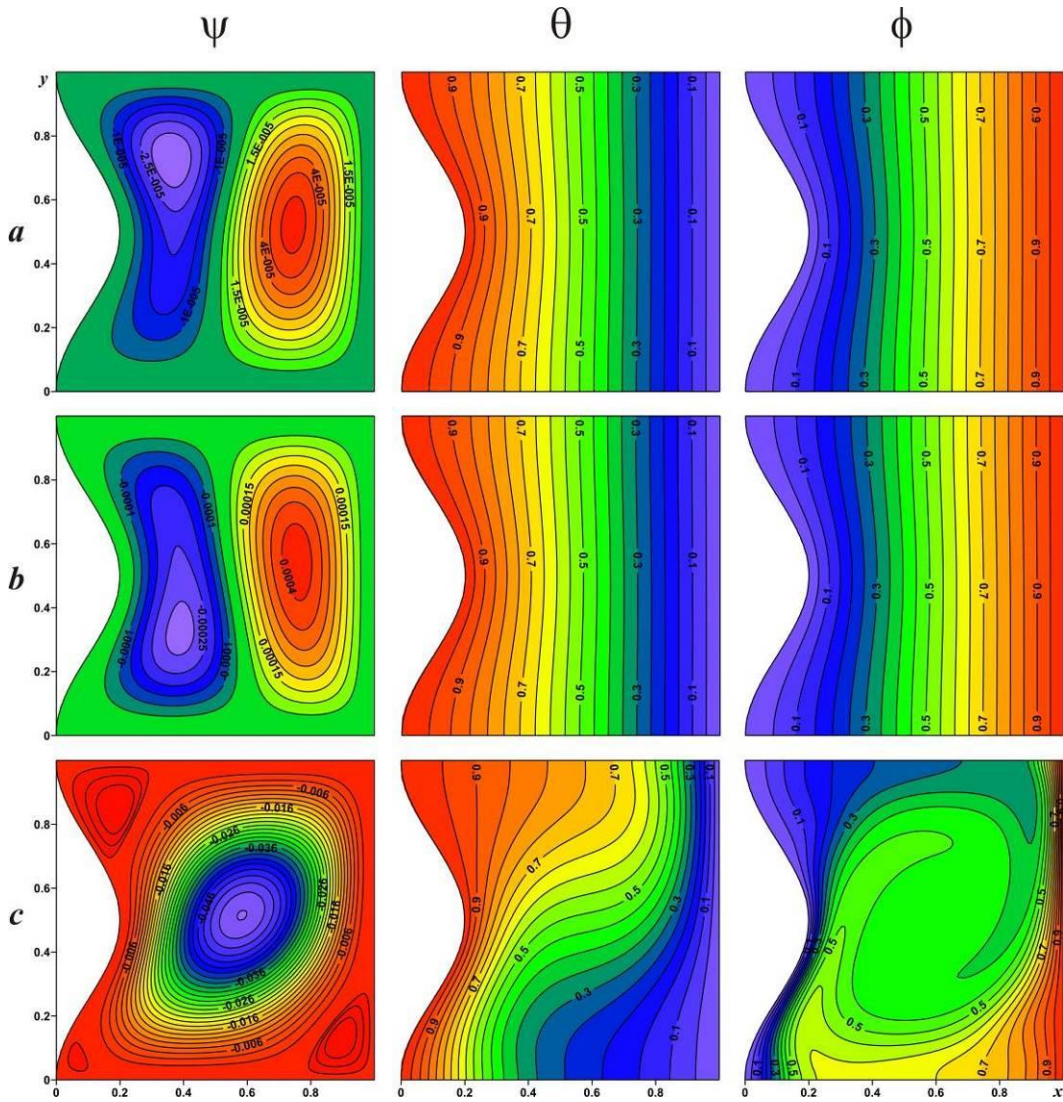


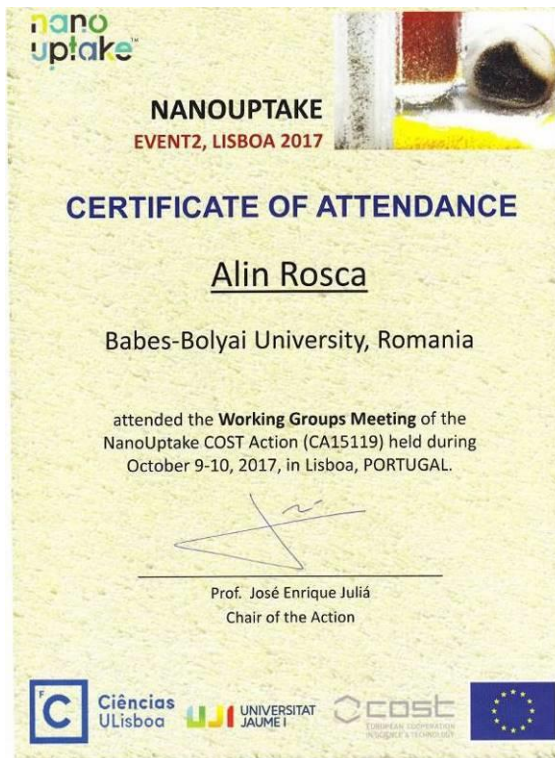
Fig. 3. Streamlines ψ , isotherms θ and isoconcentrations for case I and $\beta = 1.0$, $k_T = 0.5$, $\kappa = 1$:

$$Sc = 0.1 - a, Sc = 1.0 - b, Sc = 10.0 - c$$

Figure 3 present distributions of streamlines, isotherms and isoconcentrations inside the wavy cavity in the case of different boundary conditions and for various values of Schmidt number. It should be noted that used boundary conditions reflect the effect of wavy wall on deposition and ablation of small particles at curved wall.

For $Sc = 0.1$ and $Sc = 1.0$ one can find a domination of heat and mass diffusion mechanism when isothermal and isoconcentrations are parallel to vertical walls of constant temperature and concentration. Moreover, taking into account the thermophoresis effect the small particles are distributed uniformly inside the cavity.

Conferences



Alin Roşca, Participant NANOUPTAKE COST ACTION (CA15119), Event 2, Working Groups Meeting, WG.1 Heating, Faculty of Sciences, University of Lisbon, Portugal, 9-10 October 2017.

Title of the presentation:

MHD oblique stagnation-point flow for a Boussinesqian nanofluid past a stretching/shrinking sheet using Buongiorno's model

In this work, the MHD oblique stagnation-point flow of a Boussinesqian nanofluid past an impermeable stretching/shrinking sheet is investigated using the mathematical nanofluid model proposed by Buongiorno. The governing partial differential equations are assimilated first into ordinary differential equations then solved numerically with a `bvp4c` function in MATLAB. The numerical integration shows that if the parameter λ is negative, i.e. if λ is a shrinking parameter, then the problem admits dual solutions in a certain range of λ and the solution does not exist if λ is less than some critical value. These results are in agreement with the theoretical results of Brighi. It

seems that Merkin is the first who find the presence of multiply solutions for the problem of mixed convection flow past a vertical flat plate embedded in a porous medium.

The influence of the governing parameters on the velocity, temperature, concentration, skin friction coefficient and the local Nusselt and Sherwood numbers are analyzed graphically. Our contribution is organized as follows. In Section 2 we formulate the problem. Section 3 is devoted to some physical and analytical considerations on the solutions of the problem. Section 4 discusses the results obtained by numerical integration. In particular, we underline the influence of λ and M on the flow with careful attention to the dual solutions and the thickness of the boundary layer.



Natalia Roşca, Participant at NANOUPTAKE COST ACTION (CA15119), Event 2, Working Groups Meeting, WG. 1 Heating, Faculty of Sciences, University of Lisbon, Portugal, 9-10 October, 2017.

Title of the Presentation

Axisymmetric rotational stagnation point flow impinging radially a permeable stretching/shrinking surface in a nanofluid using Tiwari and Das model

The present work is concerned with the extension of the paper by Weidman upon the axisymmetric rotational stagnation point flow impinging on a radially stretching sheet from the case of a viscous fluid to the case of a water based nanofluid by using the mathematical nanofluid model proposed by Tiwari and Das. In addition, we have studied also the case of a shrinking sheet. A similarity transformation is used to reduce the system of governing nonlinear partial differential equations to a system of ordinary differential equations, which is then solved numerically using the function `bvp4c` from Matlab. It is found that dual (upper and lower branch) solutions exist for some values of the governing parameters. From the performed stability analysis for the dual solutions, it is found that

the upper branch solution is stable, and physically realizable, while the lower branch solution is unstable, and hence physically not realizable. Also, sample velocity and temperature profiles along both solution branches are graphically presented.

References

- J. Buongiorno, Convective transport in nanofluids, *ASME J. Heat Transfer* 128 (2006) 240-250.
- S.U.S. Choi, S. Enhancing Thermal Conductivity of Fluids with Nanoparticles, *Development and Applications of Non-Newtonian Flows*, D.A. Siginer and H.P. Wang, eds., ASME, New York, MD-Vol. 231 and FED-Vol. 66, pp. 99–105, 1995.
- C.J. Ho, W.K. Li, Y.S. Chang, C.C. Lin, Natural convection heat transfer of alumina-water nanofluid in vertical square enclosures: An experimental study, *Int. J. Thermal Sci.* 49 (2010) 1345–1353.
- O. Mahian, A. Kianifar, S.A., Kalogirou, I. Pop, S. Wongwises, A review of the applications of nanofluids in solar energy, *Int. J. Heat Mass Transfer* 57 (2013) 582–594 .
- T.G. Myers, H. Ribera, V. Cregan, Does mathematics contribute to the nanofluid debate?, *Int. J. Heat Mass Transfer* 111 (2017) 279–288.
- D.A. Nield, A. Bejan, *Convection in Porous Media* (4th ed.), Springer, New York, 2013.
- M.Z. Saghir, A. Ahadi, A. Mohamad, S. Srinivasan, Water aluminum oxide nanofluid benchmark model, *Int. J. Thermal Sciences* 109 (2016) 148–158.
- A. Sheremet, M. Sheremet, I. Pop, *Convective Flow and Heat Transfer from Wavy Surfaces: Viscous Fluids, Porous Media and Nanofluids*, CRC Press, Taylor & Francis Group, New York 2016.
- M.A. Sheremet, I. Pop, Natural convection in a wavy porous cavity with sinusoidal temperature distributions on both side walls filled with a nanofluid: Buongiorno's mathematical model, *ASME J. Heat Transfer* 137 (2015) 072601-072601-8.
- M.A. Sheremet, T. Grosan, I. Pop, Free convection in shallow and slender porous cavities filled by a nanofluid using Buongiorno's model, *ASME J. Heat Transfer* 136 (2014) Art. No. 082501.
- M.A. Sheremet, T. Grosan, I. Pop, Free convection in a square cavity filled with a porous medium saturated by nanofluid using Tiwari and Das' nanofluid model, *Transport Porous Media* 106 (2015) 595–610.